**Supplementary Online Material**

**Analytical methods**

Provided that exhumation related to subduction initiation removes at least 2-3 km of material, then it may be detected using low temperature thermochronometry. Such techniques yield cooling ages which can be interpreted to reflect the approximate time that a particular rock has passed through the closure temperature of the particular mineral system. Here we rely on helium and fission track ages in apatite. The closure temperature of helium in apatite is roughly 70 ºC (*1*), while the approximate annealing temperature of fission tracks in apatite is slightly higher [~ 105 ± 20 ºC (*2, 3*)]. Given a nominal geothermal gradient in the 20-30 ºC/km range and a 5 ºC surface temperature, exhumation from depths of ~2-3 km ought to be accompanied by cooling from above temperatures ~70 ºC, and so should be recorded by helium cooling ages in apatite. More denudation (say, of order 4-5 km) may be detected using fission track cooling ages in apatite. Comparing pairs of helium and fission track cooling ages for samples from similar elevations across Fiordland provides an indication of whether differential uplift and exhumation has occurred (e.g. tilting or folding or migration of uplift). Age pairs from samples collected over a range of elevations provide similar information, as well as insight into the time intervals during which exhumation may have accelerated in response to uplift and first-order limits on the rate of exhumation.

We obtained age apatite helium and fission track age pairs for samples from vertical elevation profiles adjacent to central Doubtful Sound and Lake Hauroko, and at Percy Saddle, as well as two transects at sea level along Dusky and Doubtful Sounds, and one lake-level transect along the North Fiord of Lake Te Anau. In addition to these

results, we also obtained helium ages for 3 samples from Milford and Georges Sound, both at sea level and at elevation [Fig. 1].

The apatite fission track data that we report here are a subset of a larger data set obtained by Peter Kamp (*4*). Apatite fission track ages and track lengths were measured at Waikato University (*5*). All fission track ages were determined using the zeta calibration method (*6*). Dosimeter glass SRM 612 was used for apatite and CN1 for zircon. Details about calibration techniques and dosimeter glasses are reported by Green (*6*).

Helium ages were obtained at the Caltech Noble Gas Laboratory using methods described by House and others (*7, 8*). Each reported age is the average computed from multiple single crystal aliquots of apatite. The 2 sigma error is computed from the average standard error (9.1%) (*9*): 2 sigma error = 2*(9.1%)*(average age)/√(N) where N is the number of replicates for each sample. The average grain-radius of the samples analyzed is 61 microns, corresponding to a closure temperature of 75 ºC, assuming a linear cooling rate of 10 ºC/my (*1*). Errors reported for the helium ages reflect the 2 sigma standard error of all of the samples in this study (*9*). Additional analytical details and results are shown in Tables S1-S3 (helium) and Tables S4, S5, S6 and S7 (apatite fission track).

**Description of results**

*Vertical transects*

Apatite helium and fission track ages obtained for six samples from central Doubtful Sound that span 773 meters elevation [Fig. 1] are shown in Figure 2a. Helium ages increase with elevation, ranging from 1.3-3.8 Ma [Table S1], while fission track

ages from the same rocks are older, typically ranging from 3.3-5.3 Ma [Table S4]. One exception, the lowest elevation sample (8901-33), yields an fission track age of 10 ± 4 Ma that falls well off of the trend defined by other samples therefore we omit it from further discussion. The fission track data show no systematic variation with elevation and track lengths measured in five samples from this profile are 14.5-15.93 microns, indicating rapid exhumation at ~4.5 ± 0.9 Ma (the average age of the transect). The larger age range in the helium ages suggests that cooling slowed somewhat as samples cooled through the helium partial retention zone (*10*) after ~3 Ma.

Eight samples from a vertical profile spanning 1183 meters on the southern side of Lake Hauroko [Fig. 1] yield helium ages that are generally positively correlated with elevation, ranging between 6.4 and 10.4 Ma [Table S1]. Corresponding fission track ages are older than the helium ages at elevations >1000 m, but are the same within 2 sigma uncertainty at low elevations [Table S5]. Fission track ages for two samples, 232 and 237, fall well off of the profile defined by the other samples, yielding much older ages [Fig. 2].

Two samples from Percy Saddle (241 and 1402 meters) yield fission track ages that are the same within 2 sigma analytical uncertainty (3.6 and 2.0 Ma, respectively; [Table S6]), indicating rapid cooling of this profile at ~2.6 ± 1.1 Ma (the average age of the samples). Corresponding helium ages (3.2 and 4.6 Ma) are the same within uncertainty as the fission track ages [Table S1], further indicating rapid cooling at ~3 Ma.

The helium age of one sample (P58924) from the head of George Sound at ~1000 m above sea level is 2.6 Ma [Fig. 2; Table S2]. No fission track ages were obtained for this sample, nor are there any other samples along this elevation transect.

*Sea level transects.*

Overall, apatite fission track ages from sea level and lake level transects are younger to the north [Fig. 3], but exhibit no significant east-to-west variation [Fig. 1], either within or among transects [Tables S4, S5, S6]. Cooling ages from Doubtful Sound range from 3.9-6.5 Ma and are similar to those from northern Lake Te Anau (2.1-6.9 Ma). Apatite fission track ages from Dusky Sound (8.5-14.2 Ma) are significantly older than the more northerly transects.

Apatite helium ages are systematically younger than or the same as apatite fission track ages from the same rocks and show the same pattern of younger ages to the north [Table S3; Fig. 3]. From south to north: helium ages from Dusky Sound (5-14 Ma) are the same within uncertainty as corresponding apatite fission track ages, as are helium ages from Doubtful Sound (6.1-3.1 Ma), while ages from Lake Te Anau are younger (0.9-3.2 Ma) than corresponding fission track ages. Helium ages from Milford Sound (1.5-3.1 Ma), for which no fission track ages are available, are similar in range to those from Lake Te Anau. The helium data also show a general trend toward younger ages to the east, both within and among the sample transects, that is not observed in the apatite fission track data. The general trend toward younger helium ages in the east is clearly apparent despite local variations in helium ages that fall outside the 2 sigma estimated uncertainty of the helium ages. It is possible that some of this local variability derived from unrecognized faults that run subparallel to the Fiordland coast and may have some recent (post-3 Ma) vertical offset.

The pattern of younger ages to the east may reflect renewed exhumation there relative to the west, or east side up tilting of the Fiordland block. However, in light of the

uncertainties in the effects of local structures on local helium ages within a given transect, as well as the large uncertainties in the apatite fission track cooling ages (apatite fission track), we cannot fully evaluate the significance of age variability within a particular transect. Despite this uncertainty, a clear trend toward younger ages to the north is apparent in both helium and fission track data and in the average ages from each transect. Therefore, we simplify the discussion by referring to average ages for each transect as outlined in the text [Fig. 3].

**Thermal models of cooling ages**

As a guide to interpret our geochronological results in terms of denudation, we reproduced the age-elevation profiles with forward models. These models were based on the *Pecube* finite element code (*11*) in which the surface temperature is imposed on a realistic finite-amplitude surface topography that changes with time. The final state of all models was the actual, present day topography of small sub-domains within Fiordland taken from the New Zealand Institute of Geological & Nuclear Sciences 50 meter digital elevation model of New Zealand [Fig. 1]. We used the code of Ehlers (*12*) to compute apatite helium and apatite fission track ages for points at the surface. We then obtained the thermal history of these points from the finite element calculation and computed the ages for all points near the observed age-elevation profiles.

For all of the models, relief did not change as a function of model time [i.e. steady-state topography]. While this is probably unlikely in Fiordland, particularly given the potentially important effects of Late Cenozoic glaciation, we find that our models are largely insensitive to topography.

Surface thermal boundary conditions are derived from a 5 x 2.5 km patch of topography centered on the Hauroko profile and a 3 x 4 km patch centered on the Doubtful Sound profile (see figure S.1). We do not know what the geothermal gradient is for Fiordland, so we used two end-member geothermal gradients, 20 ºC/km and 30 ºC/km, which are reasonable for a wide range of conditions on continents [Fig. 4]. The surface temperature for all models was taken to be 5 ºC. All other model parameters are shown in Table S.7. An example calculation in which the observed apatite helium and apatite fission track ages versus elevation profiles for Doubtful Sound were matched is shown in Fig. S.1. In this figure, the curves shown in the temperature and exhumation panels [Fig. S.1.B,C] are for the highest and lowest elevation samples in each profile and were calculated assuming a geothermal gradient of 25 ºC/km (note that Fig. 4 shows the time-temperature and time-depth histories for the highest elevation sample, computed using 20 ºC/km and 30 ºC/km geothermal gradients)**.**

**Supporting text**

**Geology of Fiordland**

Fiordland is a topographically elevated region adjacent to the Pacific-Australian plate boundary offshore of the southwestern coast of New Zealand's South Island [Fig. 1]. Rising sharply to the west of the Te Anau basin, Fiordland extends as a more or less structurally continuous block to the west coast of the South Island. The region is bounded on the north by the confluence of the Alpine and Hollyford faults and to the east by the Hollyford fault system (*13*). The western limits are delineated by the offshore Alpine fault and Fiordland subduction zone [Fig. 1].

The basement geology of Fiordland can be divided into three tectonically juxtaposed blocks that provide some insight into the uplift history of Fiordland before Late Cenozoic times (*14, 15*). North of Dusky Sound, high-grade metamorphic rocks originating at crustal depths of about 30 km [including the Western Fiordland Orthogneiss; (*16*)] are adjacent to an eastern belt of lower grade high level, intrusive rocks (*13*). Differential exhumation of these terranes may have occurred shortly after peak metamorphism (*17*). The metamorphic grade and exposure level of basement rocks also decreases significantly to the south of Dusky Sound, suggesting that a significant fault-the Dusky fault-underlies this waterway (*13*). Because this structure follows the fiord, its nature is not well understood,but it clearly places lower grade rocks to the south adjacent to higher grade rocks to the north (*13*). Granitoid intrusive rocks and low-grade metasediments south of Dusky Sound are overlain by unmetamorphosed Cretaceous to Tertiary sediments, including Oligocene submarine canyon and fan deposits and chalk marls (*13, 18, 19*).

Relative plate motions across this segment of the Pacific-Australian plate boundary changed from transtensional to transpressional during Oligocene times (*18, 20-24*) resulting in uplift of the Fiordland block (*19, 25-27*). Increased convergence was predominantly accommodated onshore by faulting along the Fiordland margins [summarized by (*19, 27, 28*)] as well as localized faulting within Fiordland (*29, 30*). Young K-Feldspar $^{40}Ar/^{39}Ar$ cooling ages from north of the Dusky Sound region indicate that structures like the Dusky Fault was active as recently as ~15 Ma (*13, 30, 31*).

As convergence again increased between the Pacific and Australian plates beginning at ~12 Ma, subduction initiated offshore and to the south of Fiordland along the Fiordland and Puysegar trench segments of the plate boundary (*22, 32, 33*). Onshore, increased convergence resulted in continued uplift of Fiordland (*19, 26, 27, 34-36*). To the north, increased transpression along the Alpine fault during this time induced the initiation of topographic growth of the South Alps (*37-39*).

**Description of the gravity anomaly**

The Fiordland gravity anomaly is characterized by a nearly 200 mGal positive Bouguer anomaly striking parallel to the Australia-Pacific plate margin with a corresponding offshore negative free-air anomaly that is similar in shape but opposite in sign (*40, 41*). Along strike, the positive gravity anomaly is centered to the south of the deepest seismicity (*42, 43*). However, any association between seismicity and gravity must be interpreted with caution as there is some debate as to the origin of the anomaly: it has been suggested that the high gravity is due to displacement upward of the Moho (*24*) or to high density rocks in the upper crust (*17*). The coincidence of the southern extent of the positive gravity anomaly with the boundary between high-grade

metamorphic rocks and low-grade metamorphic rocks around Dusky Sound supports the latter explanation. However, the magnitude of the positive anomaly cannot be explained by density contrasts associated with these rocks alone (*32*), suggesting that uplift of Fiordland may also being a contributing factor, although the timing of this uplift remains debated [e.g. (*17, 32*)].

**Discussion of denudation histories**

The results of our thermal models are summarized in Fig. 4. Note that the following estimates of denudation will increase if a lower geothermal gradient is assumed and will decrease if a higher value is used [Fig. 4]. Several regions were not explicitly modelled (Lake Te Anau, Georges Sound, Milford Sound, Percy Saddle, and Dusky Sound) because we lacked samples over a range of elevations needed to complete the modelling.

Our thermal models indicate that the helium and fission track ages from Doubtful Sound are best reproduced by 2 episodes of denudation: one at ~6 Ma in which at least 2.5 km of material was removed, followed by removal of at least an additional 1.5 km of overburden at ~1.5 Ma (note these values may be as high as 4.5 and 2.5 km, respectively). Cooling ages from George Sound, Lake Te Anau, Percy Saddle and Milford Sound are consistent with the results for Doubtful Sound, suggesting that the results from this region may be extrapolated to the others [Fig. 4].

In contrast, we observe only one episode of denudation in southern Fiordland. At Lake Hauroko, this episode occurs between ~8.5 and 6.5 Ma. The range of apatite fission track and helium age pairs, combined with shorter fission track lengths for high elevation samples at Lake Hauroko, suggest that rapid exhumation of this region initiated

no earlier than ~8.5 Ma. Likewise, zircon fission track ages and K-feldspar $^{40}Ar/^{39}Ar$ ages from the Dusky region (*31*), as well as apatite helium and fission track age pairs from Dusky Sound, indicate that rapid cooling of the region initiated no earlier than ~11 Ma. The thermal models for Lake Hauroko and cooling ages for Dusky Sound limit the amount of exhumation during this episode to ~2.5 km, with no more than ~6 km of exhumation since ~11 Ma in either place.

The thermochronologic evidence for more pronounced exhumation in northern Fiordland relative to that in the south that we infer from our data is consistent with deeper exposure levels outcropping at the surface today (*13*). However, differential uplift after 11 Ma cannot fully explain the range in exposure levels as a significant portion occurred before this time. For example, variations in K-feldspar $^{40}Ar/^{39}Ar$ cooling ages across the Dusky Fault indicate that it, and faults like it in the Breaksea Sound region to the south, may have accommodated differential uplift as late as ~15 Ma, in response to increased convergence at roughly this time (*19, 31*). However, despite an overall decrease in cooling ages to the north, we observe no significant break in either apatite fission track or helium ages across the Dusky Fault, indicating that this structure is either no younger than Late Middle Miocene in age or motion across it induced little or no denudation after this time. Moreover, apatite fission track and helium age pairs from southern Fiordland indicate that this region cooled slowly prior to ~11 Ma. Thus, the denudation episode that we detect in this region beginning at ~11 Ma is distinct from the episode recorded by K-feldspar results.

**Gravity and Uplift**

The amount of surface uplift experienced by a region like Fiordland is the product of dynamic support (in this case related to subduction initiation) and crustal thinning through denudation. Assuming the simple crustal model in Fig. S.2, the total surface uplift, $\delta h$, is a function of the amount of dynamically maintained support (or uplift), $u$, and the amount of crustal thinning, $\delta t$:

$$\delta h = \left( \frac{\rho_m - \rho_c}{\rho_m} \right) \delta t + u \qquad \text{S.1}$$

where $\delta h = h_2 - h_1$ and $\delta t = t_2 - t_1$; $\rho_c$ and $\rho_m$ are the densities of the upper crust and mantle, respectively. The lower crust is assumed to be the same for the two columns, therefore the lower crustal thicknesses and densities do not appear in eqn. S.2. The dynamically maintained support, $u$, directly results from the normal stress as $u = \sigma_{zz}/(\rho_m g)$ in air or $\sigma_{zz}/(\rho_m - \rho_w)$ in water. This dynamic uplift results in a free air gravity anomaly because the mass anomaly associated with the deflection of the Moho is not isostatically compensated by an oppositely signed mass anomaly. Consequently, we can estimate $u$ from the part of the gravity field due to dynamic uplift, $\delta g$. Assuming the Bouguer gravity formula (the gravitational attraction of a layer of thickness $\delta h$ which extends off to infinity laterally):

$$u = \frac{\delta g}{2\pi G \rho} \qquad \text{S.2}$$

where $G$ is the universal gravitational constant and $\rho$ the density of the uncompensated layer. (Here, the use of the Bouguer formula leads to an underestimate of $u$ from $\delta g$ since the anomalous mass layers are at depth and of only finite width.) Because the deflection of both the Moho and the interface between the lower and upper crust is the same ($u$), the density, $\rho$, which appears in eqn. S.2 represents the density difference between mantle and upper crust. Consequently, eqn. S.1 becomes:

S.3

$$\delta h = \left( \frac{\rho_m - \rho_c}{\rho_m} \right) \delta t + \frac{\delta g}{2\pi G(\rho_m - \rho_c)}$$

The anomalous gravity signature of Fiordland may originate from two sources (*24*). The first is a normal ocean-continent edge effect which is observed at any, isostatically balanced, passive margin. In the case of a water-covered margin, the free air gravity is low on the ocean side of the boundary and high on the continental side. A substantial fraction of the gravity (+100 mGal onshore and -100 mGal offshore) in Fiordland can be explained by this effect, while the remaining approximately +50 mGal onshore residual can be attributed to stresses within the lithosphere which tilt the Moho upward (*24*). If these stresses were to relax, Fiordland would subside 1-2 km and be topographically equivalent to the Campbell Plateau.

Using equation S.3 and nominal values for $\rho_c$ and $\rho_m$ typically reported for Fiordland [e.g. (*17, 32, 44*)], we can evaluate whether the observed values of crustal thinning and surface uplift in Fiordland are mutually consistent with one another given the amount of dynamic support predicted by existing models of subduction initiation [Fig. S.3]. From the thermochronometric results, we estimate $\delta t$ is within the 2-3 km range, but may be as great as 6 km (see Fig. 3, main text). Analysis of the evolving sedimentary record within the southern part of the South Island suggests that much of Fiordland was near sea level during the Miocene (*19*). Provided that in the Miocene the surface elevation of Fiordland was at 0 ± 500 meters, then the surface elevation, $\delta t$, has increased by 1500 ± 500 meters since that time. These values encompass a region consistent with a dynamic support of about 2 km which would be predicted for the +50 mGal residual gravity anomaly [Fig. S.3]. Thus, the amount of denudation we infer based on thermochronometric data is

consistent with our simple dynamic force balance, suggesting that the present-day dynamic support which is evident in both the Fiordland gravity anomaly and the high average elevation of the region today are likely to have the same origin as the period of accelerated denudation.

**Alternative sources of uplift**

Other sources of uplift may also contribute to the pattern of cooling ages that we observe. The slab beneath Fiordland has been described as folded downward (*42, 45*) or torn (*32, 46, 47*), which may influence patterns of uplift. For example, increased resistance to subduction of the Australian plate due to impingement into a thick, strong continental lithosphere below Otago, east of Fiordland may play a role in driving uplift (*42*). A seismic P-wave tomographic inversion beneath Fiordland indicates the Fiordland slab has encountered increased resistance to subduction and is being forced to descend vertically by a strong and thick lithospheric root to the east. In plan view, this deflection is manifested as a sharp bend in the AUS slab which is localized between Doubtful and Dusky Sounds (*42*). Because the thick lithospheric root moves with the Pacific plate, the point of downward deflection of the Australian plate would be fixed relative to the overriding plate. If this deflection produced uplift, it would be centered over the point of deflection and northward. Although no predictions of uplift have been made based on this type of model (*42*), one might expect uplift to propagate northward overtime if Fiordland responded to this uplift rigidly (that is with no faulting or folding). This model may therefore explain the enhanced erosion that we detect in the Doubtful Sound region and north relative to that in the south. It may also explain the northward progression that we observe in cooling ages.

Alternatively, delayed and enhanced uplift and exhumation in northern Fiordland may reflect crustal thickening and deformation accommodated within the Fiordland block as convergence progresses across this segment of the Australian-Pacific plate boundary. However, geological relationships indicate that most Late Cenozoic deformation has been localized along the eastern Fiordland margins (*19, 27*) and modern geodetic data indicates that most of the convergence across southern Fiordland is accommodated by relative motion offshore of Fiordland (*48*). While shortening accommodated across northern Fiordland may reflect the increased role of transpressional deformation related to the confluence of the Alpine and Hollyford faults to the north. Where similar restraining geometries occur in other transpressional settings [e.g. the eastern San Gabriel Mountains in southern California], high rates of denudation and enhanced exhumation have been reported (*49*). If this is the case, then these effects must be separated from uplift forces related to subduction initiation. However, there is little evidence in the way of crustal thickening or downward deflection of the Moho in Fiordland like that seen in the South Alps (*39*) to the north, and patterns of cooling ages appear to be very different. Examination of the thermochronologic history of northern Fiordland with respect to that of the South Alps may offer an opportunity to discriminate between these effects.

**Table S1. Helium ages for apatites from elevation transects, Central Fiordland**

| Elevation (m) | Sample | Age[C] (Ma) | [U] (ppm) | [Th] (ppm) | U/Th | [$^4$He] (nmol/g) | $F_t$ | radius (μm) | Ave.age (Ma) (2 σ) |
|---|---|---|---|---|---|---|---|---|---|
| *Percy Saddle* | | | | | | | | | |
| 244 | 8901-53 | 3.1[f] | 16.2 | 35.9 | 0.45 | 0.334 | 0.81 | 64 | 3.2(0.4) |
| | | 3.3[f] | 15.2 | 33.2 | 0.46 | 0.323 | 0.79 | 59 | |
| 1402 | 8901-62 | 4.1[f] | 14.0 | 18.4 | 0.76 | 0.320 | 0.79 | 57 | 4.6(0.6) |
| | | 5.2[f] | 14.2 | 14.4 | 0.99 | 0.371 | 0.75 | 49 | |
| *Doubtful Sound* | | | | | | | | | |
| 323 | 8901-33 | 1.0 | 2.7 | 22.6 | 0.12 | 0.032 | 0.72 | 51 | 1.3(0.1) |
| | | 1.4 | 0.7 | 14.7 | 0.05 | 0.024 | 0.78 | 66 | |
| | | 1.6 | 3.0 | 24.1 | 0.12 | 0.061 | 0.82 | 80 | |
| 463 | 8901-34 | 1.9[f] | 13.2 | 40.0 | 0.33 | 0.171 | 0.72 | 42 | 1.9(0.2) |
| | | 1.7 | 10.4 | 40.3 | 0.26 | 0.144 | 0.76 | 60 | |
| | | 2.0 | 9.8 | 38.8 | 0.25 | 0.158 | 0.78 | 66 | |
| | | 1.8 | 3.5 | 34.0 | 0.10 | 0.089 | 0.78 | 71 | |
| 616 | 8901-35 | 2.7 | 11.8 | 39.5 | 0.30 | 0.269 | 0.86 | 109 | 3.0(0.3) |
| | | 2.6 | 11.7 | 42.7 | 0.27 | 0.241 | 0.77 | 60 | |
| | | 2.9 | 9.7 | 31.4 | 0.31 | 0.216 | 0.81 | 80 | |
| | | 3.7 | 15.3 | 47.5 | 0.32 | 0.447 | 0.83 | 84 | |
| 768 | 8901-36 | 2.9 | 8.7 | 31.4 | 0.28 | 0.191 | 0.76 | 61 | 2.7(0.4) |
| | | 2.6 | 1.8 | 5.8 | 0.30 | 0.037 | 0.82 | 83 | |
| 939 | 8901-37 | 3.9 | 14.4 | 46.5 | 0.31 | 0.370 | 0.69 | 44 | 3.8(0.5) |
| | | 3.8 | 7.6 | 22.4 | 0.34 | 0.202 | 0.76 | 59 | |
| 1096 | 8901-38 | 3.6[f] | 17.5 | 55.0 | 0.32 | 0.411 | 0.70 | 41 | 3.5(0.3) |
| | | 3.5 | 18.5 | 56.3 | 0.33 | 0.449 | 0.75 | 53 | |
| | | 3.8[f] | 14.9 | 43.7 | 0.34 | 0.398 | 0.77 | 53 | |
| | | 3.3 | 15.2 | 38.3 | 0.40 | 0.336 | 0.76 | 61 | |
| | | 3.2 | 12.0 | 36.0 | 0.33 | 0.290 | 0.83 | 86 | |
| *Lake Hauroko* | | | | | | | | | |
| 777 | 8901-232 | 6.5 | 11.4 | 5.5 | 2.07 | 0.310 | 0.69 | 41 | 7.5(1.0) |
| | | 8.5 | 10.6 | 4.5 | 2.38 | 0.409 | 0.76 | 58 | |
| 640 | 8901-233 | 7.2 | 7.8 | 10.2 | 0.77 | 0.272 | 0.69 | 42 | 7.5(1.0) |
| | | 7.8 | 9.0 | 19.7 | 0.45 | 0.429 | 0.74 | 55 | |
| 457 | 8901-234 | 6.6 | 5.2 | 7.3 | 0.72 | 0.165 | 0.66 | 39 | 6.6(0.7) |
| | | 6.5 | 2.6 | 3.5 | 0.75 | 0.089 | 0.73 | 49 | |
| | | 6.8 | 1.1 | 1.2 | 0.91 | 0.040 | 0.77 | 60 | |
| 335 | 8901-235 | 6.0 | 11.2 | 4.4 | 2.52 | 0.316 | 0.79 | 67 | 6.4(0.8) |
| | | 6.8 | 10.4 | 5.7 | 1.82 | 0.326 | 0.75 | 54 | |
| 1021 | 8901-236 | 10.4 | 15.4 | 7.0 | 2.22 | 0.670 | 0.70 | 45 | 10.4(1.9) |
| | | 19.2* | 12.1 | 9.4 | 1.29 | 1.086 | 0.73 | 52 | |
| 1173 | 8901-237 | 9.4 | 56.4 | 19.0 | 2.96 | 2.368 | 0.76 | 57 | 10.4(1.3) |
| | | 11.4 | 22.4 | 6.8 | 3.32 | 1.196 | 0.80 | 73 | |
| 1344 | 8901-238 | 8.9 | 17.8 | 47.3 | 0.38 | 1.126 | 0.80 | 71 | 7.9(0.8) |
| | | 6.5 | 2.7 | 3.8 | 0.70 | 0.110 | 0.87 | 104 | |
| | | 8.2 | 16.2 | 33.1 | 0.49 | 0.886 | 0.83 | 81 | |
| 1518 | 8901-239 | 8.5 | 16.4 | 20.3 | 0.81 | 0.760 | 0.78 | 63 | 8.5(1.1) |
| | | 8.4 | 13.4 | 17.6 | 0.76 | 0.666 | 0.83 | 84 | |

[f]Samples outgassed using a vacuum furnace (*50*); all others outgassed and analyzed following method of House et al. (*7*). [C]Ages are corrected using alpha ejection factor ($F_t$) (*51*). *Excluded from average age calculation.

**Table S2. Helium ages for apatites from sea-level transects, Northern Fiordland**

| Sample | Easting | Northing | Elev. (m) | Age[C] (Ma) | [U] (ppm) | [Th] (ppm) | U/Th | [4He] (nmol/g) | Ft | radius (μm) | Ave. Age (Ma) (2 σ error) |
|---|---|---|---|---|---|---|---|---|---|---|---|
| *Milford & George Sounds* | | | | | | | | | | | |
| P58924 | 2076880 | 5561900 | 1000 | 2.6 | 15.7 | 0.5 | 33.11 | 0.179 | 0.79 | 59 | 2.6(0.3) |
| | | | | 2.5 | 13.0 | 0.3 | 40.68 | 0.143 | 0.81 | 62 | |
| P57103 | 2101970 | 5609900 | 0 | 1.5 | 2.7 | 2.8 | 0.94 | 0.017 | 0.64 | 33 | 1.5(0.3)[n] |
| P57098 | 2104290 | 5608110 | 30 | 3.1 | 0.9 | 0.1 | 14.48 | 0.012 | 0.77 | 53 | 3.1(0.6) |

All samples are outgassed using a resistance furnace. Samples provided by A. Tulloch. [C]Ages are corrected using alpha ejection factor ($F_t$) (*51*). [n]Single replicate age used

**Table S3. Helium ages for apatites from sea-level transects, Central and Southern Fiordland**

| Sample | Age[C] (Ma) | [U] (ppm) | [Th] (ppm) | U/Th | [4He] (nmol/g) | Ft | radius (μm) | Ave. Age (Ma) (2 σ error) |
|---|---|---|---|---|---|---|---|---|
| *Dusky Sound (0 meters)* | | | | | | | | |
| 8901-13 | 8.3 | 36.8 | 7.9 | 4.68 | 1.240 | 0.71 | 46 | 8.9(1.1) |
| | 9.4 | 33.5 | 7.0 | 4.80 | 1.340 | 0.75 | 55 | |
| 8901-15 | 8.0 | 4.5 | 8.3 | 0.54 | 0.193 | 0.69 | 41 | 7.3(0.9) |
| | 6.7 | 2.4 | 5.7 | 0.41 | 0.101 | 0.75 | 55 | |
| 8901-16 | 13.1 | 9.1 | 1.2 | 7.74 | 0.538 | 0.80 | 70 | 14.0(1.8) |
| | 14.8 | 10.5 | 1.9 | 5.60 | 0.660 | 0.75 | 55 | |
| 8901-19 | 8.8 | 5.4 | 1.3 | 4.16 | 0.232 | 0.85 | 97 | 9.8(1.3) |
| | 10.9 | 12.2 | 2.1 | 5.85 | 0.578 | 0.77 | 58 | |
| 9701-174 | 5.2 | 37.5 | 12.5 | 3.00 | 0.754 | 0.66 | 39 | 5.2(0.7) |
| | 5.2 | 27.2 | 13.4 | 2.02 | 0.625 | 0.72 | 49 | |
| *Doubtful Sound (0 meters)* | | | | | | | | |
| 8901-23 | 6.1[f] | 20.1 | 56.3 | 0.36 | 0.890 | 0.81 | 66 | 6.1(0.8) |
| | 6.2[f] | 20.2 | 49.4 | 0.41 | 0.873 | 0.81 | 64 | |
| 8901-24 | 4.9[f] | 57.1 | 80.9 | 0.71 | 1.629 | 0.81 | 63 | 4.8(0.6) |
| | 4.6[f] | 57.5 | 86.5 | 0.67 | 1.568 | 0.80 | 61 | |
| 8901-27 | 3.3[f] | 11.4 | 39.9 | 0.29 | 0.306 | 0.82 | 70 | 3.3(0.4) |
| | 3.3[f] | 7.6 | 27.2 | 0.28 | 0.194 | 0.76 | 53 | |
| 8901-29 | 16.5[f] | 26.9 | 91.6 | 0.29 | 3.494 | 0.80 | 61 | 14.9(1.6) |
| | 13.7 | 19.7 | 67.8 | 0.29 | 2.156 | 0.82 | 78 | |
| | 14.4 | 17.8 | 56.8 | 0.31 | 2.048 | 0.84 | 93 | |
| 8901-30 | 3.1[f] | 13.0 | 12.5 | 1.04 | 0.212 | 0.79 | 59 | 3.1(0.4) |
| | 3.1[f] | 14.6 | 15.0 | 0.97 | 0.261 | 0.85 | 83 | |
| *Lake Te Anau (200 meters)* | | | | | | | | |
| 8901-172 | 1.9 | 93.3 | 142.4 | 0.7 | 0.974 | 0.76 | 59 | 1.9(0.2) |
| | 1.9 | 86.3 | 131.5 | 0.7 | 0.893 | 0.72 | 50 | |
| 8901-174 | 1.5 | 11.1 | 24.5 | 0.5 | 0.101 | 0.75 | 57 | 1.5(0.2) |
| | 1.5 | 22.4 | 48.0 | 0.5 | 0.200 | 0.71 | 49 | |
| 8901-176 | 3.6 | 12.5 | 13.3 | 0.9 | 0.245 | 0.81 | 76 | 2.4(0.3) |
| | 1.3 | 14.1 | 9.4 | 1.5 | 0.089 | 0.76 | 56 | |
| 8901-181 | 4.3 | 6.3 | 9.8 | 0.6 | 0.156 | 0.77 | 61 | 3.2(0.4) |
| | 2.1 | 5.3 | 6.6 | 0.8 | 0.062 | 0.81 | 74 | |
| 8901-182 | 1.6 | 14.9 | 33.6 | 0.4 | 0.147 | 0.73 | 51 | 1.8(0.2) |
| | 1.9 | 10.2 | 33.3 | 0.3 | 0.147 | 0.78 | 70 | |
| | 1.8 | 21.9 | 39.6 | 0.6 | 0.238 | 0.76 | 58 | |
| 8901-185 | 1.9 | 14.8 | 48.3 | 0.3 | 0.194 | 0.72 | 49 | 1.5(0.2) |
| | 1.2 | 6.9 | 23.1 | 0.3 | 0.060 | 0.75 | 56 | |
| 8901-186 | 1.7 | 29.7 | 56.3 | 0.5 | 0.275 | 0.70 | 43 | 1.8(0.2) |
| | 1.8 | 18.5 | 47.4 | 0.4 | 0.227 | 0.77 | 63 | |
| 8901-187 | 0.7 | 5.6 | 12.4 | 0.5 | 0.023 | 0.69 | 44 | 0.9(0.1) |
| | 1.1 | 5.0 | 9.5 | 0.5 | 0.035 | 0.78 | 63 | |

[f]Samples outgassed using a vacuum furnace (*8*); all others outgassed and analyzed following method of House et al (*7*). [C]Ages are corrected using alpha ejection factor ($F_t$) (*51*).*Excluded from average age calculation.

**Table S4. Apatite fission track data for elevation transects, Central & Southern Fiordland**

| Sample | Easting/Northing | Elev. (m) | # xls | Spontaneous $\rho_s$ | Spontaneous $N_s$ | Induced $\rho_i$ | Induced $N_i$ | $P(\chi^2)$ % | $\rho_d$ | $N_d$ | Age (Ma) (2σ) | Mn Track length (1σ)(μm) | Std dev. (μm) | # Lengths |
|---|---|---|---|---|---|---|---|---|---|---|---|---|---|---|
| *Doubtful Sound(Malaspina Reach)* | | | | | | | | | | | | | | |
| 8901-33 | 2046016 / 5520217 | 323 | 20 | 0.014 | 10 | 0.245 | 180 | 98.6 | 1.068 | 2531 | 10.3(6.8) | - | - | - |
| 8901-34 | 2045743 / 5520121 | 463 | 20 | 0.029 | 15 | 1.381 | 717 | 99.4 | 1.062 | 2516 | 3.9(2.0) | 15.89(1.15) | 1.15 | 2 |
| 8901-35 | 2045469 / 5520116 | 616 | 20 | 0.041 | 35 | 1.409 | 1209 | 99.8 | 1.056 | 2501 | 5.3(1.8) | 14.93(0.3) | 1.08 | 13 |
| 8901-36 | 2045751 / 5519664 | 768 | 20 | 0.013 | 16 | 0.487 | 582 | 62.5 | 1.050 | 2486 | 5.0(2.6) | 15.88 | - | 1 |
| 8901-37 | 2045753 / 5519573 | 939 | 20 | 0.050 | 49 | 1.808 | 1769 | 99.7 | 1.045 | 2472 | 5.0(1.4) | 15 | - | 1 |
| 8901-38 | 2045652 / 5519118 | 1096 | 20 | 0.037 | 32 | 2.370 | 2074 | 57.4 | 1.258 | 3111 | 3.3(1.2) | 14.5 | - | 1 |
| *Percy Saddle* | | | | | | | | | | | | | | |
| 8901-53 | 2069998 / 5495976 | 244 | 20 | 0.059 | 50 | 3.105 | 2652 | 99.7 | 1.108 | 2629 | 3.6(1.0) | 14.7 | - | 1 |
| 8901-62 | 2067282 / 5499851 | 1402 | 20 | 0.004 | 62 | 2.099 | 3905 | 99.5 | 1.050 | 2491 | 2(0.8) | - | | |
| *Lake Hauroko* | | | | | | | | | | | | | | |
| 8901-232 | 2066266 / 5457919 | 777 | 20 | 0.221 | 132 | 2.126 | 1272 | 93.3 | 1.225 | 3030 | 21.8(4.2) | 13.1(0.51) | 2.48 | 24 |
| 8901-233 | 2066628 / 5458108 | 640 | 20 | 0.035 | 11 | 1.055 | 336 | 69.4 | 1.237 | 3059 | 7(4.2) | 14.33(0.26) | 0.57 | 5 |
| 8901-234 | 2066715 / 5458383 | 457 | 20 | 0.013 | 6 | 0.447 | 210 | 100.0 | 1.243 | 3073 | 6.1(5) | - | | |
| 8901-235 | 2066805 / 5458476 | 335 | 20 | 0.026 | 17 | 1.311 | 869 | 91.5 | 1.316 | 3225 | 4.4(2.2) | 15.69(0.51) | 1.02 | 5 |
| 8901-236 | 2065400 / 5457600 | 1021 | 20 | 0.049 | 18 | 1.485 | 545 | 97.9 | 1.003 | 2479 | 5.7(2.8) | 13.27(0.34) | 1.98 | 34 |
| 8901-237* | 2064535 / 5457707 | 1173 | 20 | 0.380 | 263 | 4.461 | 3084 | 3.5 | 1.249 | 3087 | 17.3(3.4) | 13.06(0.81) | 2.15 | 7 |
| 8901-238 | 2063448 / 5457140 | 1344 | 17 | 0.118 | 81 | 2.143 | 1469 | 8.9 | 1.254 | 3101 | 11.9(2.8) | 15.5 | - | 1 |
| 8901-239 | 2063179 / 5456862 | 1518 | 12 | 0.192 | 102 | 2.868 | 1526 | 67.6 | 1.260 | 3116 | 14.4(3) | 13.41(0.34) | 1.27 | 14 |

*$\rho_s/\rho_i$ (1σ) =0.077(0.0007)

**Table S5. Apatite fission track data for Doubtful Sound sea-level transect, Central Fiordland**

| Sample | Easting/Northing | # xls | Spontaneous $\rho_s$ | Spontaneous $N_s$ | Induced $\rho_i$ | Induced $N_i$ | $(\chi^2)$ %P | $\rho_d$ | $N_d$ | Age (Ma) (2σ) | Mn Track length (1σ)(μm) | Std dev. (μm) | # Lengths |
|---|---|---|---|---|---|---|---|---|---|---|---|---|---|
| 8901-23 | 2035100 / 5528244 | 20 | 0.067 | 43 | 2.368 | 1526 | 99.6 | 1.116 | 2647 | 5.5(1.8) | 14.69(0.47) | 0.93 | 4 |
| 8901-24 | 2036791 / 5525535 | 20 | 0.201 | 141 | 7.489 | 5252 | 70.3 | 1.110 | 4632 | 5.2(1.0) | 14.33(0.14) | 1.22 | 81 |
| 8901-27 | 2042010 / 5519508 | 20 | 0.027 | 54 | 1.121 | 2271 | 99.5 | 1.092 | 2589 | 4.5(1.2) | 14.86(0.73) | 1.03 | 3 |
| 8901-29 | 2048541 / 5516791 | 20 | 0.055 | 53 | 2.680 | 2594 | 99.6 | 1.086 | 2574 | 3.9(1.0) | 15.28(0.33) | 0.33 | 2 |
| 8901-30* | 2051345 / 5513096 | 15 | 0.084 | 52 | 3.159 | 1962 | 3.5 | 1.094 | 2705 | 5.4(2.0) | 15.3 | - | 1 |

*$\rho_s/\rho_i$ (1σ) =0.031(0.005). Elevations are zero meters.

**Table S6. Apatite fission track data for Dusky Sound sea-level transect, Southern Fiordland**

| Sample | Easting/Northing | # xls | Spontaneous | | Induced | | $P(\chi^2)$ % | $\rho_d$ | $N_d$ | Age (Ma) (2σ) | Mn Track length (1σ)(μm) | Std dev. (μm) | # Lengths |
|---|---|---|---|---|---|---|---|---|---|---|---|---|---|
| | | | $\rho_s$ | $N_s$ | $\rho_i$ | $N_i$ | | | | | | | |
| 8901-13 | 2021433 / 5473864 | 20 | 0.149 | 98 | 2.928 | 1923 | 97.5 | 1.032 | 2449 | 9.2(2.0) | 13.67(0.3) | 1.63 | 29 |
| 8901-15 | 2014534 / 5471555 | 25 | 0.044 | 36 | 0.550 | 448 | 100.0 | 1.018 | 2415 | 14.2(5.0) | 14.52(0.29) | 0.71 | 6 |
| 8901-16 | 2012446 / 5470880 | 20 | 0.120 | 86 | 1.997 | 1429 | 94.9 | 1.140 | 2705 | 12.0(2.8) | 14.21(0.23) | 1.07 | 21 |
| 8901-19a | 2014610 / 5472469 | 14 | 0.048 | 21 | 0.996 | 434 | 96.8 | 1.127 | 2676 | 9.5(4.2) | - | - | - |
| 9701-174 | 2042200 / 5480800 | 20 | 0.019 | 26 | 0.712 | 966 | 99.9 | 1.818 | 4311 | 8.5(3.4) | - | - | - |

All elevations are zero meters.

**Table S.7 Apatite fission track data for Lake Te Anau transect, northern Fiordland**

| Sample | Easting/Northing | # xls | Spontaneous | | Induced | | $P(\chi^2)$ % | $\rho_d$ | $N_d$ | Age (Ma) (2σ) | Mn Track length (1σ)(μm) | Std dev. (μm) | # Lengths |
|---|---|---|---|---|---|---|---|---|---|---|---|---|---|
| | | | $\rho_s$ | $N_s$ | $\rho_i$ | $N_i$ | | | | | | | |
| 8901-172 | 2092901/5565155 | 19 | 0.089 | 33 | 9.799 | 3615 | 20.9 | 1.369 | 3451 | 2.1(0.8) | 14.90(0.47) | 1.48 | 11 |
| 8901-174 | 2093693/5561698 | 20 | 0.032 | 26 | 2.106 | 1693 | 41.1 | 1.403 | 3469 | 3.7(1.4) | - | - | - |
| 8901-176 | 2094833/5559251 | 20 | 0.049 | 34 | 1.402 | 979 | 99.6 | 1.142 | 2709 | 6.9(2.4) | 13.98(0.54) | 1.21 | 6 |
| 8901-181 | 2099473/5555131 | 20 | 0.001 | 11 | 0.062 | 521 | 99.5 | 1.152 | 2731 | 4.2(2.6) | - | - | - |
| 8901-182 | 2099564/5555133 | 20 | 0.060 | 40 | 2.016 | 1345 | 6.4 | 1.155 | 2739 | 6.0(2.0) | 13.67(0.67) | 1.5 | 6 |
| 8901-185 | 2100668/5554695 | 20 | 0.024 | 23 | 1.837 | 1754 | 99.8 | 1.164 | 2762 | 2.7(1.2) | - | - | - |
| 8901-186 | 2100944/5554609 | 20 | 0.065 | 42 | 3.417 | 2205 | 98.9 | 1.167 | 2769 | 3.9(1.2) | 12.88(0.59) | 0.59 | 2 |
| 8901-187 | 2102040/5554628 | 16 | 0.026 | 18 | 0.988 | 690 | 98.6 | 1.171 | 2777 | 5.3(2.6) | - | - | - |

All elevations are 200 meters.

**Table S.8 Variables used for local models**

| Variable | Doubtful Sound | Lake Hauroko |
|---|---|---|
| *Size:* $L_x \cdot L_y \cdot L_z$ | 2.73km x 3.89km x 20 km | 4.64 km x 2.60 km x 20 km |
| *Grid Points:* $N_x \cdot N_y \cdot N_z$ | 22 x 22 x 22§ | 37 x 15 x 22§ |
| $\langle dT/dz \rangle$ | 20-30º C/km | 20-30º C/km |
| $\langle T \rangle$ *surface* | 5ºC | 5ºC |
| $H$ | $9 \times 10^{-13}$ ºC/s$^2$ | $9 \times 10^{-13}$ ºC/s$^2$ |
| $\kappa$ | 0.8 m/s$^2$ | 0.8 m/s$^2$ |
| Apatite grain size (μm) | 65 | 60 |

§ Resolution checks were done for select models with $N_z$ 44 and 66

**Supporting References**


1. K. A. Farley, *J. Geophys. Res.* (2000).

2. P. F. Green *et al.*, *Chem. Geol.* **79**, 155 (1989).

3. A. J. W. Gleadow, I. R. Duddy, P. F. Green, J. F. Lovering, *Contrib. Mineral. Petrol.* **94**, 405 (1986).

4. Kamp, manuscript in preparation

5. P. J. J. Kamp, P. F. Green, S. H. White, *Tectonics* **8**, 169 (1989).

6. P. F. Green, *Chem. Geol.* **58**, 1 (1985).

7. M. A. House, K. A. Farley, D. Stockli, *Earth Planet. Sci. Lett.* **183**, 365 (2000).

8. M. A. House, K. F. Farley, B. P. Kohn, *Earth Planet. Sci. Lett.* **170**, 463 (1999).

9. K. F. Farley, M. E. Rusmore, S. W. Bogue, *Geology* **29**, 99 (2001).

10. R. A. Wolf, K. F. Farley, D. M. Kass, *Chem. Geol.* **148**, 105 (1998).

11. J. Braun, *Comput. Geosci.* (submitted).

12. T. A. Ehlers, Ph.D., University of Utah (2001).

13. G. J. H. Oliver, J. H. Coggon, *Tectonophysics* **54**, 253 (1979).

14. G. J. H. Oliver, D. M. Fountain, in *Exposed cross-sections of the continental crust; proceedings* M. H. Salisbury, Ed. (D. Reidel Publishing Company, Dordrecht-Boston, 1990) 43-69.

15. G. J. H. Oliver. (Department of Scientific and Industrial Research (DSIR) Wellington New Zealand (NZL), 1980).

16. J. M. Mattinson, D. L. Kimbrough, J. Y. Bradshaw, *Contrib. Mineral. Petrol.* **92**, 383 (1986).

17. P. J. J. Kamp, K. A. Hegarty, *Geophys. J. R. Astron. Soc.* **96**, 33 (1989).

18. R. M. Carter, R. J. Norris, *Earth Planet. Sci. Lett.* **31**, 85 (1976).

19. I. M. Turnbull *et al.*, "Cretaceous and Cenozoic sedimentary basins of western Southland, South Island, New Zealand" (Tech. Rep. 1, Institute of Geological & Nuclear Sciences (N.Z.), Lower Hutt, 1993).

20. P. Molnar *et al.*, *Science* **286**, 516 (1999).

21. P. Molnar, T. Atwater, J. Mammerickx, S. M. Smith, *Geophys. J. R. Astron. Soc.* **40**, 383 (1975).

22. R. I. Walcott, *Rev. Geophys.* **36**, 1 (1998).

23. P. J. J. Kamp, *Tectonophysics* **121**, 225 (1986).

24. M. Broadbent, F. J. Davey, R. I. Walcott, "The Fiordland seismic refraction survey, 1974-5" (Tech. Rep. 124, New Zealand Department of Scientific and Industrial Research, Geophysics Division, Lower Hutt, 1978).

25. R. Sutherland, *N. Z. J. Geol. Geophys.* **39**, 251 (1996).

26. R. J. Norris, I. M. Turnbull, in *South Pacific sedimentary basins. Sedimentary basins of the World, 2* P. F. Ballance, Ed. (Elsevier Science Publishers B.V., Amsterdam, 1993) 251-270.

27. R. J. Norris, R. M. Carter, I. M. Turnbull, *J. Geol. Soc. Lond.* **135**, 191 (1978).

28. R. J. Norris, P. O. Koons, A. F. Cooper, *J. Struct. Geol.* **12**, 715 (1990).

29. A. Melhuish, R. Sutherland, F. J. Davey, G. Lamarche, *Tectonophysics* **313**, 335 (1999).

30. C. M. Ward, *J. R. Soc. N. Z.* **18**, 1 (1988).

31. C. Davids, Ph.D., Australian National University (1999).

32. F. J. Davey, E. G. C. Smith, *Geophys. J. R. Astron. Soc.* **72**, 23 (1983).

33. J.-Y. Collot *et al.*, *Geology* **23**, 519 (1995).

34. D. Smale, *J. R. Soc. N. Z.* **21**, 151 (1991).

35. R. Sutherland, *Geology* **22**, 327 (1994).

36. R. Wood, R. Herzer, R. Sutherland, A. Melhuish, *N. Z. J. Geol. Geophys.* **43**, 289 (2000).

37. J. M. Tippett, P. J. J. Kamp, *J. Geophys. Res.* **98**, 16 (1993).

38. P. J. J. Kamp, P. F. Green, J. M. Tippett, *Tectonics* **11**, 98 (1992).

39. G. E. Batt, J. Braun, *Geophys. J. Int.* **136**, 403 (1999).

40. D. J. Woodward, *N. Z. J. Geol. Geophys.* **15**, 22 (1972).

41. W. I. Reilly, A. Doone. (Department of Scientific and Industrial Research, Wellington, 1972).

42. D. Eberhart-Phillips, M. Reyners, *Geophys. J. Int.* **146**, 731 (2001).

43. H. Anderson, T. Webb, J. Jackson, *Geophys. J. Int.* **115**, 1032 (1993).

44. R. I. Walcott, *Geophys. J. R. Astron. Soc.* **52**, 137 (1978).

45. D. A. Christoffel, W. J. M. Van der Linden, *Ant. Res. Series* **19**, 235 (1972).

46. J.-F. Lebrun, G. Lamarche, J.-Y. Collot, J. Delteil, *Tectonics* **19**, 688 (2000).

47. J.-F. Lebrun, G. D. Karner, J.-Y. Collot, *J. Geophys. Res.* **103**, 7293 (1998).

48. C. Pearson, *Geophys. Res. Lett.* **25**, 3185 (1998).

49. A. E. Blythe, D. W. Burbank, K. A. Farley, E. J. Fielding, *Basin Res.* **12**, 97 (2000).

50. M. A. House, B. P. Wernicke, K. A. Farley, T. A. Dumitru, *Earth Planet. Sci. Lett.* **151**, 167 (1997).

51. K. F. Farley, R. A. Wolf, L. T. Silver, *Geochim. Cosmochim. Acta* **60**, 4223 (1996).

**Figure Captions for Supporting Figures**

**Figure S.1** A three-dimensional thermal model with denudation for a small area around the Malaspina Reach area of Doubtful Sound where we have an age-elevation profile [Fig. 1]. (A) The location map is in local model coordinates (in km) and shows the present day topography (from New Zealand 50 m DEM). Two points are shown by stars on the topographic map: star "H" near the summit peak and star "L" sea level along the fiord. The boundary conditions are set by the topography (unchanging over the 8 My duration of the experiment) and parameters listed in Table S.8. Model helium and fission track ages are computed points spaced at 0.2 km within the patch indicated by square inset. (B) The denudation and thermal history for each of the points in (A). Denudation (upper panel) is represented as effective depth vs. time where effective depth = burial depth + modern elevation of reference point above sea level. Corresponding thermal histories of points L and H are computed using the parameters in Table S.8. This model has all of the same parameters indicated in the text, except that the temperature at the base of the crust was set to 505 ºC, corresponding to an average present day geothermal gradient of 25º C/km. Note that in Fig. 4 of the main text, the curves that are shown are slightly different. They represent different denudation histories required for geothermal gradients of 30 and 20º C/km and correspond to the highest elevation rock sample analyzed (analogous to curve H). (C) Model helium and fission track ages (shown in pink) for points at the surface within the red box on the map were computed from their respective thermal histories and plotted as a function of their present day elevations. Modeled ages are shown with observed ages from this region (Doubtful Sound; Fig. 2).

**Figure S.2.** Two crustal blocks in dynamic balance in which the second block is experiencing dynamic support through a normal stress $\sigma_{zz}$. The second crustal column has a much thinner upper crust but stands at a higher elevation.

**Figure S.3.** Model of crustal thinning and dynamic uplift. The lower curves show the isostatic response of the crustal column to thinning; the upper curves show the superimposed effects of postulated 2 km of dynamic support (*u*) associated with a +50 mGal gravity anomaly (*24*). In both cases, the two green lines represent a nominal density difference of 500 kg/m$^3$. Uncertainty in the density difference is depicted with two additional values: 400 kg/m$^3$ (red lines) and 600 kg/m$^3$ (blue lines). The box labeled Doubtful is our estimate of the amount of crustal thinning deduced from thermochronology in the Doubtful Sound region and the regional surface uplift. Note that a larger crust-mantle density difference leads to a smaller change in surface elevation for a given change in crustal thickness while implying a larger amount of dynamic support.

**Fig. S.1.**

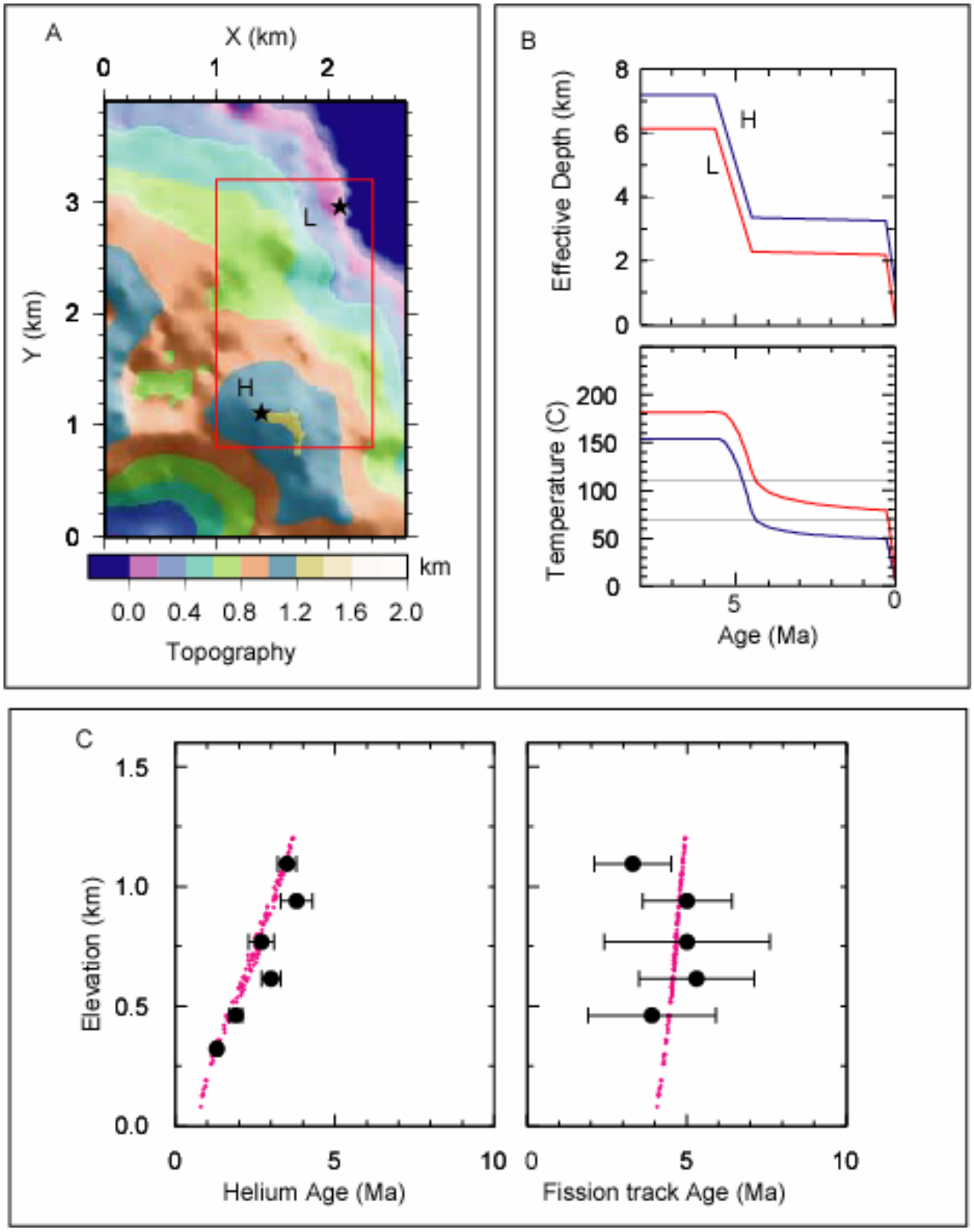
A
X (km)
0
1
2
3
Y (km)
0
1
2
L
H
km
0.0 0.4 0.8 1.2 1.6 2.0
Topography
B
Effective Depth (km)
8
6
4
2
0
H
L
Temperature (C)
200
150
100
50
0
5
0
Age (Ma)
C
Elevation (km)
1.5
1.0
0.5
0.0
0
5
10
Helium Age (Ma)
0
5
10
Fission track Age (Ma)

**Fig. S.2.**

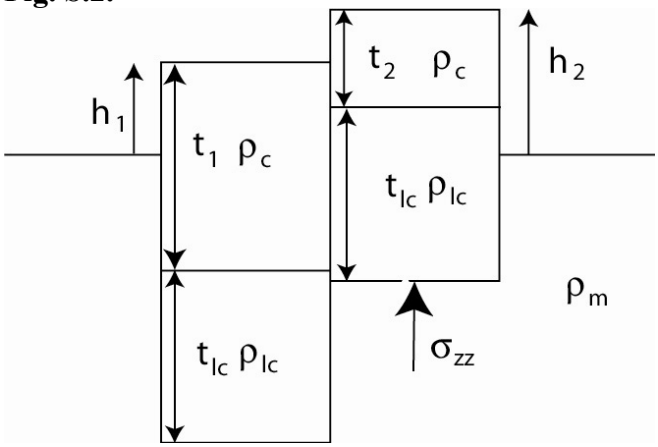
h1
t1 ρc
t2 ρc
h2
tlc ρlc
tlc ρlc
ρm
σzz

**Fig. S.3.**

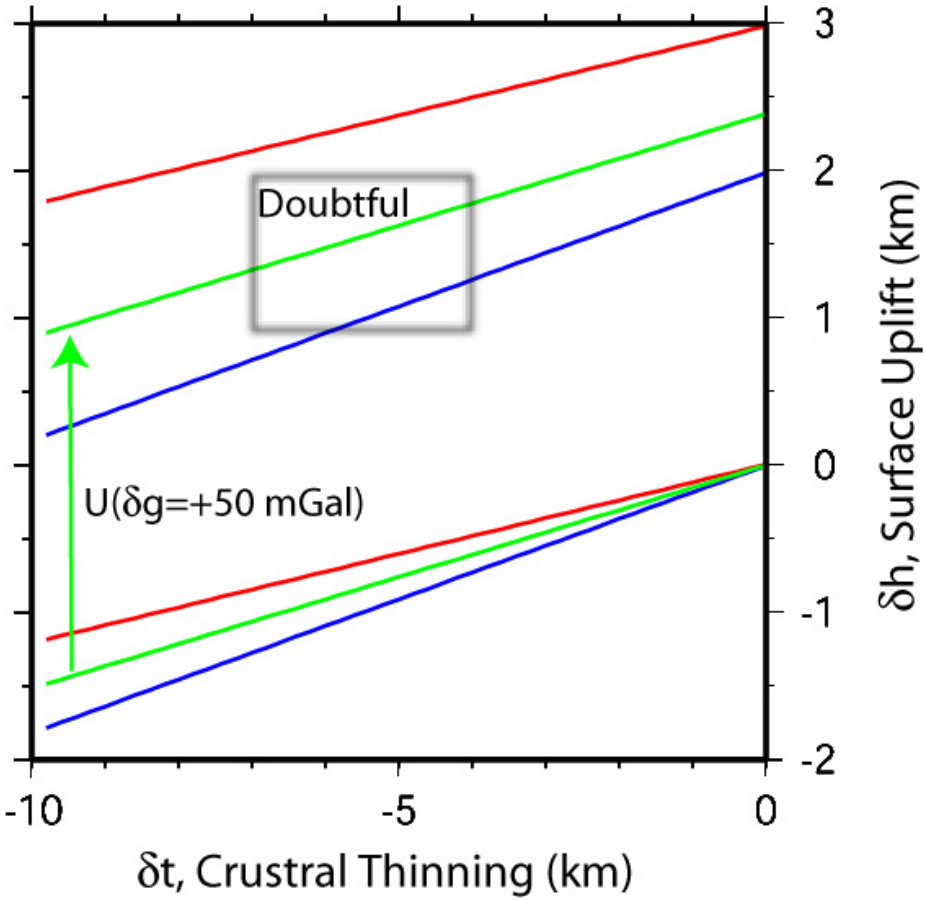
Doubtful
U(δg=+50 mGal)
3
2
1
0
-1
-2
-10
-5
0
δh, Surface Uplift (km)
δt, Crustral Thinning (km)